Geophysical Research Letters

RESEARCH LETTER
10.1029/2023GL105630

Ionospheric Plasma Density Gradients Associated With Night-Side Energetic Electron Precipitation

Xiao-Jia Zhang[1,2], Xing Meng[3], Anton V. Artemyev[2], Ying Zou[4], and Didier Mourenas[5,6]

[1]Department of Physics, The University of Texas at Dallas, Richardson, TX, USA, [2]Department of Earth, Planetary, and Space Sciences, University of California, Los Angeles, Los Angeles, CA, USA, [3]Jet Propulsion Laboratory, California Institute of Technology, Pasadena, CA, USA, [4]Johns Hopkins University Applied Physics Laboratory, Laurel, MD, USA, [5]CEA, DAM, DIF, Arpajon, France, [6]Laboratoire Matière en Conditions Extrêmes, Paris-Saclay University, CEA, Bruyères-le-Châtel, France

Key Points:

- Total electron content (TEC) maps are examined during energetic electron precipitation at the conjugate low altitude
- Night-side whistler-mode wave driven precipitation is often associated with local horizontal TEC gradients
- Night-side EMIC wave driven precipitation is often poleward of the TEC minima associated with the plasmapause projection

Supporting Information:

Supporting Information may be found in the online version of this article.

Correspondence to:

X.-J. Zhang,
xjzhang@utdallas.edu

Citation:

Zhang, X.-J., Meng, X., Artemyev, A. V., Zou, Y., & Mourenas, D. (2023). Ionospheric plasma density gradients associated with night-side energetic electron precipitation. *Geophysical Research Letters*, *50*, e2023GL105630. https://doi.org/10.1029/2023GL105630

Received 24 JUL 2023
Accepted 11 OCT 2023

Abstract Energetic electron precipitation from the equatorial magnetosphere into the atmosphere plays an important role in magnetosphere-ionosphere coupling: precipitating electrons alter ionospheric properties, whereas ionospheric outflows modify equatorial plasma conditions affecting electromagnetic wave generation and energetic electron scattering. However, ionospheric measurements cannot be directly related to wave and energetic electron properties measured by high-altitude, near-equatorial spacecraft, due to large mapping uncertainties. We aim to resolve this by projecting low-altitude measurements of energetic electron precipitation by ELFIN CubeSats onto total electron content (TEC) maps serving as a proxy for ionospheric density structures. We examine three types of precipitation on the nightside: precipitation of <200 keV electrons in the plasma sheet, bursty precipitation of <500 keV electrons by whistler-mode waves, and relativistic (>500 keV) electron precipitation by EMIC waves. All three types of precipitation show distinct features in TEC horizontal gradients, and we discuss possible implications of these features.

Plain Language Summary Bursty precipitation of energetic electrons, via pitch-angle scattering by whistler-mode waves from the magnetosphere to the ionosphere, is an important factor in the global magnetosphere-ionosphere coupling. It induces local modifications of ionospheric density and chemical composition. A recurrent problem in the investigation of this process is the presence of large uncertainties in the field-line mapping between ionospheric density structures and high altitude satellites measuring electron fluxes in the magnetosphere. In the present study, such uncertainties are significantly reduced by making use of precipitating electron fluxes recorded by ELFIN CubeSats at low altitudes (450 km) just above the ionosphere and comparing them with maps of the corresponding ionospheric density structures. We identify three different types of electron precipitation on the nightside, corresponding to low, moderate, and high energy precipitating electrons. We show that each type of the precipitation is characterized by particular plasma density gradients in the ionosphere, suggesting a key role of wave ducting by plasma density gradients in fostering the precipitation of 300–500 keV electrons by whistler-mode waves, and the potential importance of midnight plasma injections in generating EMIC waves that can further precipitate 0.5–2 MeV electrons far away from the plasmasphere.

1. Introduction

Energy and mass exchanges between the hot, rarefied magnetospheric plasma and cold, collisional ionospheric plasma is largely contributed by energetic electron precipitation driven by near-equatorial wave-particle interactions (Khazanov et al., 2018; Mukhopadhyay et al., 2022; Ni et al., 2016; Nishimura et al., 2020; Thorne et al., 2010). In response to this precipitation, secondary electrons flow out of the ionosphere (Khazanov et al., 2014) and may radically change hot electron distributions near the equator (Khazanov et al., 2015, 2019; Nishimura et al., 2015). Such a two-way coupled picture assumes certain correlations between ionospheric properties and energetic electron precipitation: precipitating electrons change the ionosphere density (e.g., Glukhov et al., 1992; Sivadas et al., 2017; Sanchez et al., 2022; Ma et al., 2022, and references therein), whereas ionospheric outflows alter the equatorial wave generation, propagation, and efficiency of energetic electron scattering and precipitation (e.g., Artemyev et al., 2020; Khazanov et al., 2015).

The main observational evidence for energetic electron precipitation affecting ionosphere characteristics has been shown by conjugate wave measurements from near-equatorial spacecraft and ionosphere properties from

incoherent scatter radars (Ma et al., 2022; Miyoshi et al., 2021; Sanchez et al., 2022), where models of ionization in response to precipitating particles further support the energetic electron impact on ionospheric properties (Fang et al., 2008; Pettit et al., 2023; Xu et al., 2020). This approach is based on the well developed models of energetic electron scattering by near-equatorial plasma waves (see reviews by Shprits et al., 2008; Ni et al., 2016; Thorne et al., 2021), but suffers from magnetic mapping uncertainties between the equator and low altitudes (Ma et al., 2022). An alternative approach is to compare low-altitude measurements of electron precipitation with ionospheric characteristics, which has been well developed for the plasma sheet electron precipitation (<30 keV) from multiple satellites of Defense Meteorological Satellite Program (Lyons et al., 2021; Mishin & Streltsov, 2021). Statistical measurements of energetic (>30 keV) electron fluxes at low altitudes, however, had long been limited to Polar Operational Environmental Satellites (POES) and Meteorological Operational (MetOp) satellites. POES/MetOp only provides energetic electron fluxes for a few integral channels (Evans & Greer, 2004; Green, 2013), and thus requires conjugate, near-equatorial wave measurements to identify the precipitation drivers (e.g., Capannolo et al., 2018, 2019; Li et al., 2013).

In this study, we introduce a new data set that enables investigations of ionosphere-magnetosphere coupling via energetic electron precipitation: low-altitude ELFIN CubeSat measurements (Angelopoulos et al., 2020). Because of their full pitch-angle resolution, ELFIN measurements enable us to separate precipitation enhancements driven by the near-equatorial electron scattering from those due to adiabatic increases of the equatorial flux. In the meantime, the good energy resolution further allows ELFIN to distinguish the three most representative types of electron precipitation patterns in the night-side inner magnetosphere: precipitation of <200 keV electrons from the plasma sheet caused by curvature scattering, bursty precipitation of <500 keV electrons by whistler-mode waves in the plasma injection region, and relativistic (>500 keV) electron precipitation by EMIC waves. Each of these precipitation types has very distinct features in the ELFIN precipitating-to-trapped flux data set, and thus can be identified without conjugate equatorial measurements. Conjugate measurements have been used to verify this identification procedure for precipitation patterns driven by different wave modes and curvature scattering (L. Chen et al., 2022; Shi et al., 2022; Grach et al., 2022; An et al., 2022; Zhang et al., 2022; Artemyev et al., 2022). We show here that each of these precipitation types can be associated with a specific structure in total electron content (TEC). As TEC variations/structures are proxies for ionospheric density variations/structures, the coupling between TEC and ELFIN measurements confirms that energetic electron precipitation significantly contributes to spatial (horizontal) gradients in the ionosphere density, especially for those electron precipitation due to curvature scattering. Moreover, gradients in the horizontal TEC, representative of ionosphere density, are known to be strongly associated with the plasma density gradients at the equatorial magnetosphere (Heilig et al., 2022; Shinbori et al., 2021; Yizengaw & Moldwin, 2005) and, thus, our results also suggest that energetic electron precipitation may be organized by the magnetosphere density gradients, especially for electron precipitation driven by whistler-mode waves. Finally, the localization of precipitation events relative to horizontal TEC gradients enables one to locate the near-equatorial region, where electrons are scattered into the loss cone by wave-particle resonant interactions or by magnetic field line curvature, relative to magnetospheric plasma boundaries, for example, particularly important for EMIC-driven precipitation.

2. Data Sets

In this study we will use two data sets: low-altitude ELFIN measurements of precipitating and locally trapped (outside the bounce loss cone) energetic electrons during the 2020 tail (nightside) season (between April and September), and total electron content (TEC) maps conjugate to the ELFIN observed precipitation. ELFIN energetic particle detector measures 50–6,000 keV electrons with 16 energy channels and 8 pitch-angle channels (Angelopoulos et al., 2020, 2023), which covers the entire 180° over one half spin (~1.5s). We average ELFIN measurements within and outside the local bounce loss cone separately to obtain the energy spectra of precipitating flux j_{prec} and trapped flux j_{trap}. TEC data trace well plasma density variations in the ionosphere (Belehaki et al., 2004; Heise et al., 2002; Lee et al., 2013), including enhanced density structures like plasmaspheric plumes (Foster et al., 2002; Walsh et al., 2014). Thus, the horizontal gradients in TEC may be interpreted as ionosphere density gradients with possible equatorial sources, for example, ion and electron precipitation, and as counterparts of equatorial density gradients (e.g., of plasmapause gradient; see Yizengaw & Moldwin, 2005; Shinbori et al., 2021; Heilig et al., 2022). Here we have used horizontal TEC maps from the Madrigal database provided by the Massachusetts Institute of Technology Haystack (http://cedar.openmadrigal.org; see Rideout and Coster (2006); Coster et al. (2013); Vierinen et al. (2015)). We use TEC measurements at 5-min resolution and

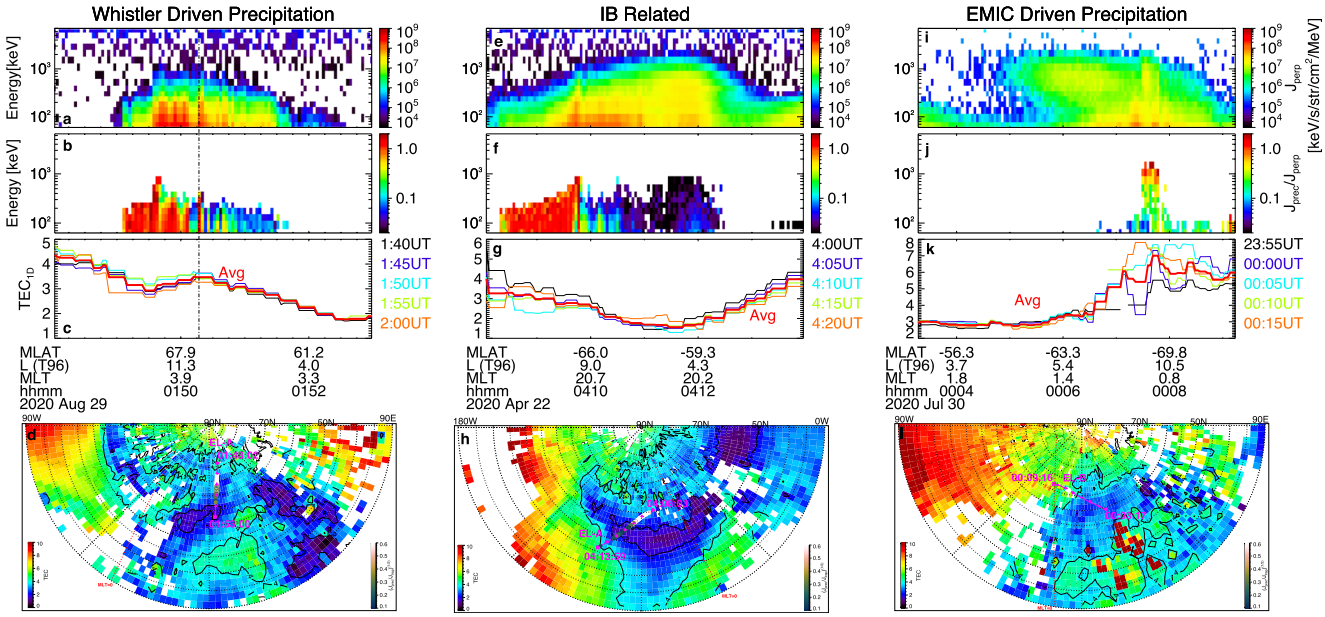

Figure 1. Three typical precipitation events observed by ELFIN, and the corresponding TEC profiles along the ELFIN track. Left, center, and right columns show precipitation driven by whistler-mode waves, plasma sheet inner boundary (isotropy boundary), and EMIC waves, respectively. Panels (a,b,e,f,i,j) show the locally trapped electron fluxes and j_{prec}/j_{trap} flux ratio from ELFIN observations, as a function of electron energy; *L*-shell of ELFIN projection with the T96 (Tsyganenko, 1995) model is shown below. Panels (c,g,k) show the average TEC profile along ELFIN's track at different times close to ELFIN observations; the red line shows the average TEC profile. Panels (d,h,l) show 2D TEC maps, with the projected ELFIN trajectory color-coded by j_{prec}/j_{trap} for 100 keV (left and center columns) and 1 MeV (right column) electrons. Diamonds and asterisks mark the start and end times of the trajectories; crosses are 1 min tickmarks. The overlaid red dotted line marks the magnetic local midnight (magnetic local time near zero). The vertical dashed line in panels (a–c) highlights one burst of whistler-mode wave driven electron precipitation at 100–500 keV.

$1 \times 1°$ spatial resolution. We further average them within $\pm 2°$ in latitude and longitude around the ELFIN orbit to obtain the corresponding 1D TEC profile.

Our ELFIN data set includes three subsets of night-side observations. The main criterion for event selection is a good TEC coverage in the magnetic local time (MLT) and *L*-shell sector of ELFIN observations. This criterion significantly reduces the corresponding data set of ELFIN measurements: events constituting each subset represent only ~10% of all events of such types measured by ELFIN in 2020.

The first subset consists of 27 events (56 bursts of precipitation) with typical features of whistler-mode driven precipitation: large j_{prec}/j_{trap} flux ratio at low energies (~50–100 keV) and decreasing j_{prec}/j_{trap} toward higher energy, with almost no precipitating flux above 1 MeV; the full list of events can be found in Table S1 in Supporting Information S1. These events were identified based on previous investigations of ELFIN measurements in conjunction with wave detection near the equator (e.g., Tsai et al., 2022; Zhang et al., 2023). These 27 events, selected based on the simultaneous TEC coverage, are similar to usual ELFIN observations of whistler-mode wave driven precipitation. Figures 1a–1d shows a typical example of such events observed in the heart of the outer radiation belt (~01:50:15UT), as marked by the vertical dashed line, earthward from the plasma sheet; the plasma sheet is observed at low altitudes (before ~01:49:30UT) as a prolonged region filled by <200 keV, isotropic ($j_{prec}/j_{trap} \sim 1$) precipitation driven by curvature scattering (Artemyev et al., 2022; Wilkins et al., 2023).

The second subset consists of 16 events with a precipitation pattern typical of the plasma sheet; the full list of events can be found in Table S2 in Supporting Information S1. The equatorial (inner) edge of such precipitation is the so-called isotropy boundary (Imhof et al., 1977; Sergeev et al., 1983; Sergeev & Tsyganenko, 1982) where a combination of curvature scattering around the equatorial current sheet and high fluxes of relativistic electrons at the outer edge of the radiation belt provides a very distinct, localized (a fraction of a degree in latitude) burst of isotropic ($j_{prec}/j_{trap} \sim 1$) electron precipitation often up to MeV (Artemyev et al., 2022; Wilkins et al., 2023); note that these 16 events, selected based on TEC coverage, are similar to usual ELFIN observations of the isotropy boundary. A typical example of the isotropy boundary observed by ELFIN is shown in Figure 1 (center column), where this boundary (at ~04:09:45UT) separates the outer radiation belt, with transient precipitation

bursts of sub-MeV electrons scattered by whistler-mode waves, and the plasma sheet, with isotropic precipitation of <200 keV electrons.

The third subset consists of five events with EMIC wave-driven precipitation: very small j_{prec}/j_{trap} at low energies ~50–300 keV, increasing j_{prec}/j_{trap} toward higher energy, approaching $j_{prec}/j_{trap} \sim 1$ at ~1 MeV, the typical minimum electron energy for cyclotron resonance with EMIC waves (see discussions of such events with ELFIN observations in conjunction with equatorial wave measurements in Grach et al., 2022; An et al., 2022). Note that these events, selected based on TEC coverage, are not different from typical events of EMIC wave-driven precipitation observed by ELFIN (see Angelopoulos et al., 2023). Figures 1i–1l shows one such EMIC-driven precipitation event in the pre-midnight sector, where EMIC waves can be generated along the drifting path of injected hot ions. The precipitation lasts for several spins (tens of seconds). This is much longer than whistler-mode wave driven precipitation bursts, which usually last only a couple of spins. This difference is likely due to the different spatial scales of the whistler-mode and EMIC wave source regions near the equator (see, e.g., Blum et al., 2016; Blum et al., 2017; Agapitov et al., 2017).

Panels (d,h,l) in Figure 1 project ELFIN orbits onto the 2D TEC distributions averaged 10 min around the precipitation. During all three events, the TEC distribution exhibits a similar pattern on the night-side: a large TEC at high latitudes due to plasma sheet precipitation and at low latitudes inside the plasmasphere (Weygand et al., 2021; Yizengaw & Moldwin, 2005), with a TEC minimum at middle latitudes. This TEC minimum corresponds to the so-called mid-latitude ionospheric trough (Carpenter & Lemaire, 2004; Vo & Foster, 2001), associated with ring current ion precipitation and the enhanced azimuthal plasma convection (Aa et al., 2020; Heise et al., 2002). The equatorial edge of this trough, where the TEC reaches a minimum, is statistically conjugate to the equatorial plasmapause location (Heilig et al., 2022; Shinbori et al., 2021; Yizengaw & Moldwin, 2005).

Panels (c, g, k) show TEC profiles along ELFIN's track within ±10 min from ELFIN measurements; the average profile is shown in red. The TEC usually decreases from the plasma sheet (at high latitudes) to a minimum value around the projection of the plasmapause (within the mid-latitude ionospheric trough), and then increases equatorward from the plasmapause. Panel (c) shows that the selected whistler-mode wave driven precipitation burst (shown by a vertical dashed line) is observed near a local maximum in TEC. Panel (g) shows that the TEC profile is relatively flat poleward of the isotropy boundary, but exhibits a strong horizontal gradient earthward from this boundary, in the outer radiation belt. Panel (k) shows that EMIC wave-driven precipitation is observed just earthward from the plasma sheet and still relatively far from the TEC minimum (at ~00:05 UT) associated with the plasmapause. In the next section, we statistically examine and discuss these different features of TEC in relation with energetic electron precipitation patterns.

3. Statistical Analysis of TEC Horizontal Gradients Related to Specific Patterns of Energetic Electron Precipitation

3.1. Whistler-Mode Wave Driven Precipitation Bursts

Figure 2 shows superposed epoch profiles of $j_{prec}/j_{trap}(\Delta MLAT)$ and TEC($\Delta MLAT$) (normalized to values at the magnetic latitude of the precipitation burst, $MLAT_0$), where $\Delta MLAT = MLAT - MLAT_0 < 0$ on the inner magnetosphere side and $\Delta MLAT > 0$ on the plasma sheet side. The flux ratio, j_{prec}/j_{trap}, exhibits a clear peak at $\Delta MLAT = 0$, and remains large up to several hundreds of keV. These events are separated into three different categories, corresponding to the presence of either (a) a horizontal TEC gradient (51%), (b) a TEC minimum (20%), or (c) a TEC maximum (29%), each recorded within ±0.5° of the magnetic latitude where a whistler wave-driven electron precipitation spike is detected by ELFIN (this ±0.5° latitude range approximately corresponds to the uncertainty in the projection of ELFIN orbit onto the TEC map). For each category, we show in Figures 2a, 2e, and 2i the average normalized TEC/TEC_0 profile, respectively centered at the middle of the maximum horizontal TEC gradient, minimum of TEC, or maximum of TEC.

In Figures 2a, 2e, and 2i, the normalized TEC shows a local minimum or maximum around the precipitation burst during half of the precipitation events, and a steeper gradient near the precipitation burst than away from it during the other events. Horizontal TEC gradients may be interpreted as ionosphere density gradients with counterparts as equatorial radial gradients of plasma density in the magnetosphere (Heilig et al., 2022; Shinbori et al., 2021; Yizengaw & Moldwin, 2005). Thus, the coexistence of whistler-mode wave driven precipitation bursts with significant horizontal TEC gradients potentially indicates wave ducting by equatorial density gradients. Such ducting would explain the presence of intense electron precipitation up to 500 keV. The night-side equatorial

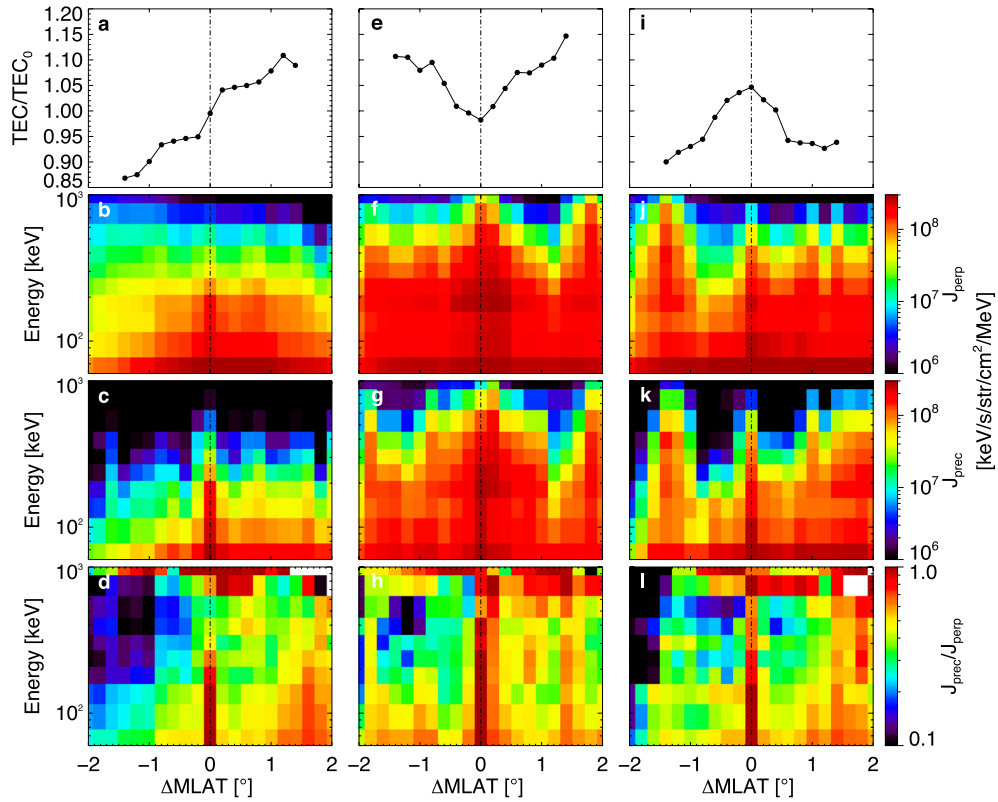

Figure 2. Superposed epoch analysis of the three different types of TEC profiles (black) observed during precipitation events detected by ELFIN. (a) Superposed epoch analysis of the maximum horizontal TEC gradient recorded along ELFIN trajectory within ±0.5° of the magnetic latitude of the whistler wave-driven electron precipitation burst, in the absence of a minimum/maximum of TEC there. (e) Same as (a) for minima of TEC within ±0.5° of the magnetic latitude of the electron precipitation burst. (i) Same as (a) for maxima of TEC. The TEC is normalized to TEC_0, the TEC level at the middle of the maximum horizontal TEC gradient, minimum of TEC, or maximum of TEC, respectively. Corresponding median distribution of the (b,f,j) locally trapped electron flux, (c,g,k) precipitating electron fluxes, and (d,h,l) precipitating-to-trapped flux ratio, plotted versus magnetic latitudes centered at the precipitation burst (see text for details).

magnetosphere in the outer radiation belt is filled by suprathermal electrons (Li et al., 2010), which can quickly damp whistler-mode waves via Landau resonance (Bortnik et al., 2007) when they become oblique while propagating away from the equator (Breuillard et al., 2012; L. Chen et al., 2013; Watt et al., 2013; Katoh, 2014). As a result, statistical observations have shown that whistler-mode waves are well confined around the equatorial plane (Agapitov et al., 2013; Meredith et al., 2012). However, near-equatorial waves cannot scatter >100 keV electrons (Artemyev et al., 2021; Gan et al., 2023), and thus observations of precipitating electrons up to 500 keV indicate the presence of another population of waves at middle latitudes on the night-side. These are likely ducted waves, which are trapped by equatorial plasma density gradients (Hanzelka & Santolík, 2019; Streltsov & Bengtson, 2020; Woodroffe & Streltsov, 2013) and can propagate to middle latitudes in the field-aligned mode with minimum Landau damping (e.g., Shen et al., 2021; R. Chen, Gao, Lu, Chen, et al., 2021; R. Chen, Gao, Lu, Tsurutani, & Wang, 2021; Ke et al., 2021). Figure 2 supports this scenario of relativistic electron bursts associated with wave ducting by equatorial plasma density gradients, as implied by the horizontal TEC gradients. An alternative, or supplementary, explanation is that energetic electron precipitation driven by whistler-mode waves can heat the ionospheric plasma and contribute to local ionosphere density variations, which may further lead to horizontal TEC gradients (Sheng et al., 2019, 2020). Such whistler-driven electron precipitation should be most intense around the minimum resonant energy, that is ~5–10 keV for whistler-mode chorus waves.

3.2. Electron Isotropy Boundary

Figure 3 shows results from the superposed epoch analysis during plasma sheet (isotropy) boundary events. ELFIN measurements clearly show a peak of j_{prec}/j_{trap} around $\Delta MLAT = 0$, and j_{prec}/j_{trap} remains ~1 for <200 keV

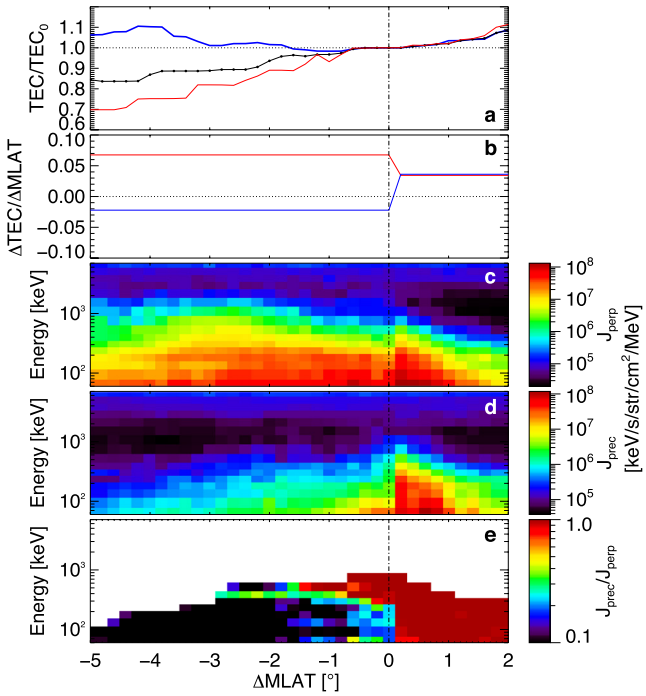

Figure 3. Superposed epoch analysis of plasma sheet electron precipitation and TEC distributions: (a) median profiles the normalized TEC along ELFIN trajectories: events with clear signatures of a mid-latitude ionospheric trough (red), events without signatures of mid-latitude ionospheric trough (blue), and for the entire data set (black), (b) ΔTEC/Δ*MLAT* gradient for the two groups of events, median distribution of the (c) locally trapped electron flux, (d) precipitating electron fluxes, and (e) precipitating-to-trapped flux ratio. Results are plotted versus magnetic latitudes centered at the boundary between the plasma sheet and the inner magnetosphere; TEC is normalized to the value at this boundary (see text for details).

electrons poleward from this peak, corresponding to plasma sheet precipitation. The formation of the mid-latitude ionospheric trough equatorward from the electron isotropy boundary is controlled by ion injections, which are responsible for ion precipitation and strong azimuthal drifts that reduce the ionosphere plasma density within the mid-latitude ionospheric trough (Carpenter & Lemaire, 2004; Rodger, 2008; Vo & Foster, 2001). Therefore, we separate isotropy boundary events into two groups: events in the first group demonstrate clear signatures of a mid-latitude ionospheric trough in 2D TEC maps, and events in the second group do not show a clear TEC minimum. Figure 3a shows TEC profiles for the first group (red), second group (blue), and for the entire data set (black), while Figure 3b shows the ΔTEC/Δ*MLAT* gradient for these two groups of events, estimated from separate linear fits to TEC profiles at $\Delta MLAT > 0$ and $\Delta MLAT < 0$. Figures 3a and 3b show that the TEC horizontal gradient is weak in the plasma sheet for both groups of events. However, the TEC horizontal gradient significantly increases in the inner magnetosphere for the first group of events, whereas it remains weak but changes sign for the second group of events. These features should be related to the different mechanisms responsible for TEC horizontal gradients in the (electron) plasma sheet and inner magnetosphere. Poleward from the isotropy boundary (within the electron plasma sheet), the TEC horizontal gradient is due to the equatorial radial variation of precipitating plasma sheet electron fluxes (predominantly at <10 keV) (see also Sivadas et al., 2019). Equatorward from this boundary (within the inner magnetosphere), energetic electron precipitation from the plasma sheet is largely reduced and the main contributions to TEC variations come from precipitation of ring current ions and ionosphere plasma transport due to electric drifts (e.g., Rodger, 2008, and references therein). Differences in equatorial radial gradients of plasma sheet electron fluxes and ring current ion fluxes may be responsible for the different horizontal TEC gradients poleward and equatorward from the electron isotropy boundary. Figure 3 demonstrates that TEC horizontal gradients can be used to infer the equatorial location of the electron isotropy boundary, the inner edge of the electron plasma sheet.

3.3. EMIC Wave-Driven Precipitation Events

Figure 4 shows four additional events of EMIC-driven relativistic electron precipitation, which share similar properties as the event from Figure 1 (right column). Relativistic electrons penetrate deep into the ionosphere down to the F-layer (Fang et al., 2008; Pettit et al., 2023; Xu et al., 2020), but their fluxes are likely too moderate to significantly alter the TEC (Miyoshi et al., 2021). Therefore, comparisons of EMIC wave-driven precipitation events with TEC horizontal gradients mainly reveal the position of the equatorial source of such precipitation relative to the plasmapause, as the plasmapause is indicated by the local TEC minimum within the mid-latitude ionospheric trough (Heilig et al., 2022; Shinbori et al., 2021; Yizengaw & Moldwin, 2005).

During all these events from Figure 4, the relativistic electron precipitation is mapped quite far from the plasmapause, but just equatorward from the inner edge of the plasma sheet, within the flow breaking region where plasma sheet injections stop (Dubyagin et al., 2011; Nakamura et al., 2009). EMIC wave-driven precipitation events projected onto TEC maps in Figures 1i–1l and Figure 4 seem to indicate a contradicting location from the EMIC wave preferred generation region in the noon/dusk plasmasphere (Jun et al., 2019, 2021), where a high-density plasma of plasmaspheric origin decreases both the resonant energy of ions (increasing the resonant ion fluxes available for EMIC generation, see Thorne & Kennel, 1971; L. Chen et al., 2009, 2011) and electrons (leading to ≤1 MeV electron precipitation, see Summers & Thorne, 2003; Drozdov et al., 2017). Therefore, the present comparison of TEC horizontal gradients with ELFIN observations reveals the presence of a new mechanism of ≤1 MeV electron precipitation in the night side (Angelopoulos et al., 2023; Capannolo et al., 2022; Kim et al., 2021).

10.1029/2023GL105630

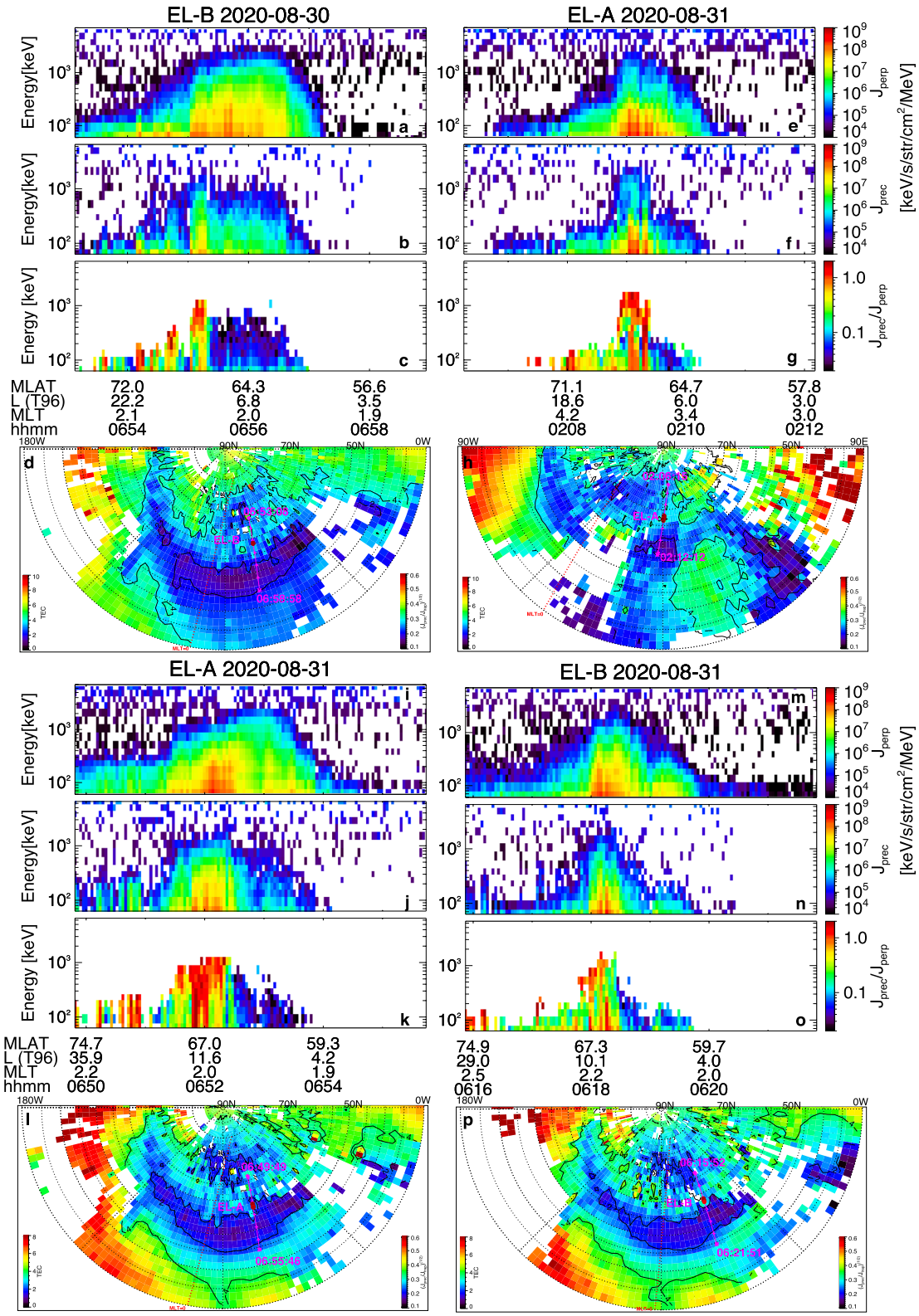

Figure 4. Four EMIC wave-driven precipitation events: ELFIN observations of (a,e,i,m) locally trapped, (b,f,j,n) precipitating electron fluxes, and (c,g,k,o) precipitating-to-trapped flux ratio. (d,h,l,p) Projection of ELFIN observations onto 2D TEC maps in the northern hemisphere; ELFIN trajectories are color-coded by the flux ratio (j_{prec}/j_{trap}) of 1 MeV electrons; diamonds and asterisks mark the start and end times of the trajectories; crosses are 1 min tickmarks. The overlaid red dotted line marks the magnetic local midnight (magnetic local time is around zero).

4. Conclusions

In this study, we have combined night-side observations of energetic electron precipitations by low-altitude ELFIN CubeSats and TEC horizontal gradient measurements to examine three types of precipitation events relative to ionosphere plasma boundaries. The main conclusions can be summarized as follows:

- Bursts of whistler-mode wave-driven electron precipitation are associated with TEC horizontal gradients. Such gradients being mapped to the equatorial magnetosphere region may indicate the presence of plasma density gradients that allow wave ducting (Streltsov & Bengtson, 2020; Woodroffe & Streltsov, 2013). This ducting can guide whistler-mode waves, allowing them to propagate without strong Landau damping up to middle latitudes (R. Chen, Gao, Lu, Chen, et al., 2021; R. Chen, Gao, Lu, Tsurutani, & Wang, 2021) where waves can scatter and precipitate several hundreds of keV electrons into the atmosphere (see discussions in L. Chen et al., 2022). This scenario of magnetosphere-ionosphere coupling may explain the association of TEC horizontal gradients with ELFIN observations of energetic electron precipitation.
- The inner edge of the electron plasma sheet (the electron isotropy boundary) coincides with a sudden change of TEC latitudinal (horizontal) gradients, with a notably stronger TEC gradient in the inner magnetosphere when signatures of a mid-latitude ionospheric trough are present. This feature clearly demonstrates the importance of electron curvature scattering, the main mechanism of electron precipitation from the magnetotail, in coupling the plasma sheet to the ionosphere (see also Sivadas et al., 2019), which enables us to locate the electron plasma sheet inner edge (isotropy boundary) from TEC horizontal gradients.
- Long-lasting EMIC wave-driven relativistic electron precipitation occurs far from the night-side plasmapause, right within the plasma injection region, slightly equatorward from the inner edge of the electron plasma sheet. Such strong losses of relativistic electrons at the outer radiation belt boundary may compete with the magnetopause shadowing mechanism (e.g., Turner et al., 2012) in depleting the radiation belt.

These examples demonstrate the high potential of using TEC data sets to investigate the localization and relative importance of energetic electron precipitation (Pettit et al., 2023), but also indicate the nonlinearity of magnetosphere-ionosphere energy and mass exchange, with ionosphere feedback to energetic electron precipitation. Such nonlinearity significantly complicates the modeling of magnetosphere-ionosphere coupling (Huang, 2021), which requires incorporating wave-induced precipitation and dynamics of cold plasma structures self-consistently in future models of wave propagation and wave-particle resonant interaction.

Data Availability Statement

ELFIN measurements are available in ELFIN data archive in CDF format (ELFIN, 2023). Data of total electron content (TEC) are provided by Massachusetts Institute of Technology Haystack via the Madrigal database (TEC, 2023); see details in Rideout and Coster (2006); Coster et al. (2013); Vierinen et al. (2015). Data analysis was done using SPEDAS V4.1 (Angelopoulos et al., 2019), which can be downloaded from (SPEDAS, 2023).

Acknowledgments
We are grateful to NASA's CubeSat Launch Initiative for ELFIN's successful launch in the desired orbits. We acknowledge early support of ELFIN project by the AFOSR, under its University Nanosat Program, UNP-8 project, contract FA9453-12-D-0285, and by the California Space Grant program. We are thankful to ELFIN's P.I., Dr. V. Angelopoulos, for valuable discussions and comments about ELFIN data and ELFIN/TEC comparisons. We also acknowledge critical contributions of numerous volunteer ELFIN team student members. A.V.A and X.-J.Z. acknowledge support from the NASA Grants 80NSSC23K0403, 80NSSC22K0522, 80NSSC21K0729, and 80NSSC23K0089. X.-J. Z. acknowledges support from the NSF Grant 2329897. Part of the research was performed at the Jet Propulsion Laboratory, California Institute of Technology, under a contract with National Aeronautics and Space Administration (80NM0018D0004).

References

Aa, E., Zou, S., Erickson, P. J., Zhang, S.-R., & Liu, S. (2020). Statistical analysis of the main ionospheric trough using swarm in situ measurements. *Journal of Geophysical Research: Space Physics*, *125*(3), e27583. https://doi.org/10.1029/2019JA027583

Agapitov, O. V., Artemyev, A., Krasnoselskikh, V., Khotyaintsev, Y. V., Mourenas, D., Breuillard, H., et al. (2013). Statistics of whistler mode waves in the outer radiation belt: Cluster STAFF-SA measurements. *Journal of Geophysical Research*, *118*(6), 3407–3420. https://doi.org/10.1002/jgra.50312

Agapitov, O. V., Blum, L. W., Mozer, F. S., Bonnell, J. W., & Wygant, J. (2017). Chorus whistler wave source scales as determined from multipoint Van Allen Probe measurements. *Geophysical Research Letters*, *44*(6), 2634–2642. https://doi.org/10.1002/2017GL072701

An, X., Artemyev, A., Angelopoulos, V., Zhang, X., Mourenas, D., & Bortnik, J. (2022). Nonresonant scattering of relativistic electrons by electromagnetic ion cyclotron waves in Earth's radiation belts. *Physical Review Letters*, *129*(13), 135101. https://doi.org/10.1103/PhysRevLett.129.135101

Angelopoulos, V., Cruce, P., Drozdov, A., Grimes, E. W., Hatzigeorgiu, N., King, D. A., et al. (2019). The space physics environment data analysis system (SPEDAS). *Space Science Reviews*, *215*(1), 9. https://doi.org/10.1007/s11214-018-0576-4

Angelopoulos, V., Tsai, E., Bingley, L., Shaffer, C., Turner, D. L., Runov, A., et al. (2020). The ELFIN mission. *Space Science Reviews*, *216*(5), 103. https://doi.org/10.1007/s11214-020-00721-7

Angelopoulos, V., Zhang, X. J., Artemyev, A. V., Mourenas, D., Tsai, E., Wilkins, C., et al. (2023). Energetic electron precipitation driven by electromagnetic ion cyclotron waves from ELFIN's low altitude perspective. *Space Science Reviews*, *219*(37), 37. https://doi.org/10.1007/s11214-023-00984-w

Artemyev, A. V., Angelopoulos, V., Zhang, X. J., Runov, A., Petrukovich, A., Nakamura, R., et al. (2022). Thinning of the magnetotail current sheet inferred from low-altitude observations of energetic electrons. *Journal of Geophysical Research: Space Physics*, *127*(10), e2022JA030705. https://doi.org/10.1029/2022JA030705

Artemyev, A. V., Demekhov, A. G., Zhang, X. J., Angelopoulos, V., Mourenas, D., Fedorenko, Y. V., et al. (2021). Role of ducting in relativistic electron loss by whistler-mode wave scattering. *Journal of Geophysical Research: Space Physics*, *126*(11), e29851. https://doi.org/10.1029/2021JA029851

Artemyev, A. V., Zhang, X. J., Angelopoulos, V., Mourenas, D., Vainchtein, D., Shen, Y., et al. (2020). Ionosphere feedback to electron scattering by equatorial whistler mode waves. *Journal of Geophysical Research: Space Physics*, *125*(9), e28373. https://doi.org/10.1029/2020JA028373

Belehaki, A., Jakowski, N., & Reinisch, B. W. (2004). Plasmaspheric electron content derived from GPS TEC and digisonde ionograms. *Advances in Space Research*, *33*(6), 833–837. https://doi.org/10.1016/j.asr.2003.07.008

Blum, L. W., Agapitov, O., Bonnell, J. W., Kletzing, C., & Wygant, J. (2016). EMIC wave spatial and coherence scales as determined from multipoint Van Allen Probe measurements. *Geophysical Research Letters*, *43*(10), 4799–4807. https://doi.org/10.1002/2016GL068799

Blum, L. W., Bonnell, J. W., Agapitov, O., Paulson, K., & Kletzing, C. (2017). EMIC wave scale size in the inner magnetosphere: Observations from the dual Van Allen Probes. *Geophysical Research Letters*, *44*(3), 1227–1233. https://doi.org/10.1002/2016GL072316

Bortnik, J., Thorne, R. M., Meredith, N. P., & Santolik, O. (2007). Ray tracing of penetrating chorus and its implications for the radiation belts. *Geophysical Research Letters*, *34*(15), L15109. https://doi.org/10.1029/2007GL030040

Breuillard, H., Zaliznyak, Y., Krasnoselskikh, V., Agapitov, O., Artemyev, A., & Rolland, G. (2012). Chorus wave-normal statistics in the Earth's radiation belts from ray tracing technique. *Annals of Geophysics*, *30*(8), 1223–1233. https://doi.org/10.5194/angeo-30-1223-2012

Capannolo, L., Li, W., Ma, Q., Chen, L., Shen, X. C., Spence, H. E., et al. (2019). Direct observation of subrelativistic electron precipitation potentially driven by EMIC waves. *Geophysical Research Letters*, *46*(22), 12711–12721. https://doi.org/10.1029/2019GL084202

Capannolo, L., Li, W., Ma, Q., Zhang, X.-J., Redmon, R. J., Rodriguez, J. V., et al. (2018). Understanding the driver of energetic electron precipitation using coordinated multisatellite measurements. *Geophysical Research Letters*, *45*(14), 6755–6765. https://doi.org/10.1029/2018GL078604

Capannolo, L., Li, W., Millan, R., Smith, D., Sivadas, N., Sample, J., & Shekhar, S. (2022). Relativistic electron precipitation near midnight: Drivers, distribution, and properties. *Journal of Geophysical Research: Space Physics*, *127*(1), e30111. https://doi.org/10.1029/2021JA030111

Carpenter, D., & Lemaire, J. (2004). The plasmasphere boundary layer. *Annales Geophysicae*, *22*(12), 4291–4298. https://doi.org/10.5194/angeo-22-4291-2004

Chen, L., Thorne, R. M., Li, W., & Bortnik, J. (2013). Modeling the wave normal distribution of chorus waves. *Journal of Geophysical Research*, *118*(3), 1074–1088. https://doi.org/10.1029/2012JA018343

Chen, L., Thorne, R. M., & Bortnik, J. (2011). The controlling effect of ion temperature on EMIC wave excitation and scattering. *Geophysical Research Letters*, *38*(16), L16109. https://doi.org/10.1029/2011GL048653

Chen, L., Thorne, R. M., & Horne, R. B. (2009). Simulation of EMIC wave excitation in a model magnetosphere including structured high-density plumes. *Journal of Geophysical Research*, *114*(A7), A07221. https://doi.org/10.1029/2009JA014204

Chen, L., Zhang, X.-J., Artemyev, A., Angelopoulos, V., Tsai, E., Wilkins, C., & Horne, R. B. (2022). Ducted chorus waves cause sub-relativistic and relativistic electron microbursts. *Geophysical Research Letters*, *49*(5), e97559. https://doi.org/10.1029/2021GL097559

Chen, R., Gao, X., Lu, Q., Chen, L., Tsurutani, B. T., Li, W., & Wang, S. (2021). In situ observations of whistler mode chorus waves guided by density ducts. *Journal of Geophysical Research: Space Physics*, *126*(4), e28814. https://doi.org/10.1029/2020JA028814

Chen, R., Gao, X., Lu, Q., Tsurutani, B. T., & Wang, S. (2021). Observational evidence for whistler mode waves guided/ducted by the inner and outer edges of the plasmapause. *Geophysical Research Letters*, *48*(6), e92652. https://doi.org/10.1029/2021GL092652

Coster, A., Williams, J., Weatherwax, A., Rideout, W., & Herne, D. (2013). Accuracy of GPS total electron content: GPS receiver bias temperature dependence. *Radio Science*, *48*(2), 190–196. https://doi.org/10.1002/rds.20011

Drozdov, A. Y., Shprits, Y. Y., Usanova, M. E., Aseev, N. A., Kellerman, A. C., & Zhu, H. (2017). EMIC wave parameterization in the long-term VERB code simulation. *Journal of Geophysical Research*, *122*(8), 8488–8501. https://doi.org/10.1002/2017JA024389

Dubyagin, S., Sergeev, V., Apatenkov, S., Angelopoulos, V., Runov, A., Nakamura, R., et al. (2011). Can flow bursts penetrate into the inner magnetosphere? *Geophysical Research Letters*, *38*(8), 8102. https://doi.org/10.1029/2011GL047016

ELFIN. (2023). Electron losses and fields investigation (ELFIN) data archive. ELFIN. [Dataset]. Retrieved from https://data.elfin.ucla.edu/

Evans, D. S., & Greer, M. S. (2004). Polar orbiting environmental satellite space environment monitor-2: Instrument description and archive data documentation.

Fang, X., Randall, C. E., Lummerzheim, D., Solomon, S. C., Mills, M. J., Marsh, D. R., et al. (2008). Electron impact ionization: A new parameterization for 100 eV to 1 MeV electrons. *Journal of Geophysical Research*, *113*(A9), A09311. https://doi.org/10.1029/2008JA013384

Foster, J. C., Erickson, P. J., Coster, A. J., Goldstein, J., & Rich, F. J. (2002). Ionospheric signatures of plasmaspheric tails. *Geophysical Research Letters*, *29*(13), 1623. https://doi.org/10.1029/2002GL015067

Gan, L., Artemyev, A., Li, W., Zhang, X.-J., Ma, Q., Mourenas, D., et al. (2023). Bursty energetic electron precipitation by high-order resonance with very-oblique whistler-mode waves. *Geophysical Research Letters*, *50*(8). https://doi.org/10.1029/2022GL101920

Glukhov, V. S., Pasko, V. P., & Inan, U. S. (1992). Relaxation of transient lower ionospheric disturbances caused by lightning-whistler-induced electron precipitation bursts. *Journal of Geophysical Research*, *97*(A11), 16971–16979. https://doi.org/10.1029/92JA01596

Grach, V. S., Artemyev, A. V., Demekhov, A. G., Zhang, X.-J., Bortnik, J., Angelopoulos, V., et al. (2022). Relativistic electron precipitation by EMIC waves: Importance of nonlinear resonant effects. *Geophysical Research Letters*, *49*(17), e99994. https://doi.org/10.1029/2022GL099994

Green, J. L. (2013). Meped telescope data processing algorithm theoretical basis document.

Hanzelka, M., & Santolík, O. (2019). Effects of ducting on whistler mode chorus or exohiss in the outer radiation belt. *Geophysical Research Letters*, *46*(11), 5735–5745. https://doi.org/10.1029/2019GL083115

Heilig, B., Stolle, C., Kervalishvili, G., Rauberg, J., Miyoshi, Y., Tsuchiya, F., et al. (2022). Relation of the plasmapause to the midlatitude ionospheric trough, the sub-auroral temperature enhancement and the distribution of small-scale field aligned currents as observed in the magnetosphere by THEMIS, RBSP, and Arase, and in the topside ionosphere by swarm. *Journal of Geophysical Research: Space Physics*, *127*(3), e29646. https://doi.org/10.1029/2021JA029646

Heise, S., Jakowski, N., Wehrenpfennig, A., Reigber, C., & Lühr, H. (2002). Sounding of the topside ionosphere/plasmasphere based on GPS measurements from CHAMP: Initial results. *Geophysical Research Letters*, *29*(14), 44-1–44-4. https://doi.org/10.1029/2002GL014738

Huang, C. (2021). Magnetospheric energy input to the ionosphere. In C. Huang & G. Lu (Eds.), *Ionosphere dynamics and applications* (Vol. 3, p. 3). https://doi.org/10.1002/9781119815617.ch1

Imhof, W. L., Reagan, J. B., & Gaines, E. E. (1977). Fine-scale spatial structure in the pitch angle distributions of energetic particles near the midnight trapping boundary. *Journal of Geophysical Research*, *82*(32), 5215–5221. https://doi.org/10.1029/JA082i032p05215

Jun, C.-W., Miyoshi, Y., Kurita, S., Yue, C., Bortnik, J., Lyons, L., et al. (2021). The characteristics of EMIC waves in the magnetosphere based on the Van Allen Probes and Arase observations. *Journal of Geophysical Research: Space Physics*, *126*(6), e29001. https://doi.org/10.1029/2020JA029001

Jun, C. W., Yue, C., Bortnik, J., Lyons, L. R., Nishimura, Y., & Kletzing, C. (2019). EMIC wave properties associated with and without injections in the inner magnetosphere. *Journal of Geophysical Research: Space Physics*, *124*(3), 2029–2045. https://doi.org/10.1029/2018JA026279

Katoh, Y. (2014). A simulation study of the propagation of whistler-mode chorus in the Earth's inner magnetosphere. *Earth Planets and Space*, *66*(1), 6. https://doi.org/10.1186/1880-5981-66-6

Ke, Y., Chen, L., Gao, X., Lu, Q., Wang, X., Chen, R., et al. (2021). Whistler mode waves trapped by density irregularities in the Earth's magnetosphere. *Geophysical Research Letters*, *48*(7), e92305. https://doi.org/10.1029/2020GL092305

Khazanov, G. V., Chen, M. W., Lemon, C. L., & Sibeck, D. G. (2019). The magnetosphere-ionosphere electron precipitation dynamics and their geospace consequences during the 17 March 2013 storm. *Journal of Geophysical Research: Space Physics*, *124*(8), 6504–6523. https://doi.org/10.1029/2019JA026589

Khazanov, G. V., Glocer, A., & Himwich, E. W. (2014). Magnetosphere-ionosphere energy interchange in the electron diffuse aurora. *Journal of Geophysical Research: Space Physics*, *119*(1), 171–184. https://doi.org/10.1002/2013JA019325

Khazanov, G. V., Robinson, R. M., Zesta, E., Sibeck, D. G., Chu, M., & Grubbs, G. A. (2018). Impact of precipitating electrons and magnetosphere-ionosphere coupling processes on ionospheric conductance. *Space Weather*, *16*(7), 829–837. https://doi.org/10.1029/2018SW001837

Khazanov, G. V., Tripathi, A. K., Sibeck, D., Himwich, E., Glocer, A., & Singhal, R. P. (2015). Electron distribution function formation in regions of diffuse aurora. *Journal of Geophysical Research*, *120*(11), 9891–9915. https://doi.org/10.1002/2015JA021728

Kim, H., Schiller, Q., Engebretson, M. J., Noh, S., Kuzichev, I., Lanzerotti, L. J., et al. (2021). Observations of particle loss due to injection associated electromagnetic ion cyclotron waves. *Journal of Geophysical Research: Space Physics*, *126*(2), e28503. https://doi.org/10.1029/2020JA028503

Lee, H. B., Jee, G., Kim, Y. H., & Shim, J. S. (2013). Characteristics of global plasmaspheric TEC in comparison with the ionosphere simultaneously observed by Jason-1 satellite. *Journal of Geophysical Research: Space Physics*, *118*(2), 935–946. https://doi.org/10.1002/jgra.50130

Li, W., Ni, B., Thorne, R. M., Bortnik, J., Green, J. C., Kletzing, C. A., et al. (2013). Constructing the global distribution of chorus wave intensity using measurements of electrons by the POES satellites and waves by the Van Allen Probes. *Geophysical Research Letters*, *40*(17), 4526–4532. https://doi.org/10.1002/grl.50920

Li, W., Thorne, R. M., Bortnik, J., Nishimura, Y., Angelopoulos, V., Chen, L., et al. (2010). Global distributions of suprathermal electrons observed on THEMIS and potential mechanisms for access into the plasmasphere. *Journal of Geophysical Research*, *115*(A12), A00J10. https://doi.org/10.1029/2010JA015687

Lyons, L. R., Nishimura, Y., Zhang, S., Coster, A., Liu, J., Bristow, W. A., et al. (2021). Direct connection between auroral oval streamers/flow channels and equatorward traveling ionospheric disturbances. *Frontiers in Astronomy and Space Sciences*, *8*, 169. https://doi.org/10.3389/fspas.2021.738507

Ma, Q., Xu, W., Sanchez, E. R., Marshall, R. A., Bortnik, J., Reyes, P. M., et al. (2022). Analysis of electron precipitation and ionospheric density enhancements due to hiss using incoherent scatter radar and Arase observations. *Journal of Geophysical Research: Space Physics*, *127*(8), e30545. https://doi.org/10.1029/2022JA030545

Meredith, N. P., Horne, R. B., Sicard-Piet, A., Boscher, D., Yearby, K. H., Li, W., & Thorne, R. M. (2012). Global model of lower band and upper band chorus from multiple satellite observations. *Journal of Geophysical Research*, *117*(A10), 10225. https://doi.org/10.1029/2012JA017978

Mishin, E. V., & Streltsov, A. (2021). Mesoscale and small-scale structure of the subauroral geospace. In C. Huang & G. Lu (Eds.), *Ionosphere dynamics and applications* (Vol. 3, p. 139). https://doi.org/10.1002/9781119815617.ch8

Miyoshi, Y., Hosokawa, S., Kurita, S.-I., Oyama, Y., Ogawa, S., Saito, I., et al. (2021). Penetration of MeV electrons into the mesosphere accompanying pulsating aurorae. *Scientific Reports*, *11*(1), 13724. https://doi.org/10.1038/s41598-021-92611-3

Mukhopadhyay, A., Welling, D., Liemohn, M., Ridley, A., Burleigh, M., Wu, C., et al. (2022). Global driving of auroral precipitation: 1. Balance of sources. *Journal of Geophysical Research: Space Physics*, *127*(7), e30323. https://doi.org/10.1029/2022JA030323

Nakamura, R., Retinò, A., Baumjohann, W., Volwerk, M., Erkaev, N., Klecker, B., et al. (2009). Evolution of dipolarization in the near-Earth current sheet induced by earthward rapid flux transport. *Annales Geophysicae*, *27*(4), 1743–1754. https://doi.org/10.5194/angeo-27-1743-2009

Ni, B., Thorne, R. M., Zhang, X., Bortnik, J., Pu, Z., Xie, L., et al. (2016). Origins of the Earth's diffuse auroral precipitation. *Space Science Reviews*, *200*(1–4), 205–259. https://doi.org/10.1007/s11214-016-0234-7

Nishimura, Y., Bortnik, J., Li, W., Liang, J., Thorne, R. M., Angelopoulos, V., et al. (2015). Chorus intensity modulation driven by time-varying field-aligned low-energy plasma. *Journal of Geophysical Research: Space Physics*, *120*(9), 7433–7446. https://doi.org/10.1002/2015JA021330

Nishimura, Y., Lessard, M. R., Katoh, Y., Miyoshi, Y., Grono, E., Partamies, N., et al. (2020). Diffuse and pulsating aurora. *Space Science Reviews*, *216*(1), 4. https://doi.org/10.1007/s11214-019-0629-3

Pettit, J., Elliott, S., Randall, C., Halford, A., Jaynes, A., & Garcia-Sage, K. (2023). Investigation of the drivers and atmospheric impacts of energetic electron precipitation. *Frontiers in Astronomy and Space Sciences*, *10*. https://doi.org/10.3389/fspas.2023.1162564

Rideout, W., & Coster, A. (2006). Automated GPS processing for global total electron content data. *GPS Solutions*, *10*(3), 219–228. https://doi.org/10.1007/s10291-006-0029-5

Rodger, A. (2008). *The mid-latitude trough—Revisited* (Vol. 181, pp. 25–33). Washington DC American Geophysical Union Geophysical Monograph Series. https://doi.org/10.1029/181GM04

Sanchez, E. R., Ma, Q., Xu, W., Marshall, R. A., Bortnik, J., Reyes, P., et al. (2022). A test of energetic particle precipitation models using simultaneous incoherent scatter radar and Van Allen Probes observations. *Journal of Geophysical Research: Space Physics*, *127*(8), e30179. https://doi.org/10.1029/2021JA030179

Sergeev, V. A., Sazhina, E. M., Tsyganenko, N. A., Lundblad, J. A., & Soraas, F. (1983). Pitch-angle scattering of energetic protons in the magnetotail current sheet as the dominant source of their isotropic precipitation into the nightside ionosphere. *Planetary and Space Science*, *31*(10), 1147–1155. https://doi.org/10.1016/0032-0633(83)90103-4

Sergeev, V. A., & Tsyganenko, N. A. (1982). Energetic particle losses and trapping boundaries as deduced from calculations with a realistic magnetic field model. *Planetary and Space Science*, *30*(10), 999–1006. https://doi.org/10.1016/0032-0633(82)90149-0

Shen, Y., Chen, L., Zhang, X.-J., Artemyev, A., Angelopoulos, V., Cully, C. M., et al. (2021). Conjugate observation of magnetospheric chorus propagating to the ionosphere by ducting. *Geophysical Research Letters*, *48*(23), e95933. https://doi.org/10.1029/2021GL095933

Sheng, C., Deng, Y., Chen, Y.-J., Heelis, R. A., & Huang, Y. (2019). Effects of alignment between particle precipitation and ion convection patterns on joule heating. *Journal of Geophysical Research: Space Physics*, *124*(6), 4905–4915. https://doi.org/10.1029/2018JA026446

Sheng, C., Deng, Y., Zhang, S.-R., Nishimura, Y., & Lyons, L. R. (2020). Relative contributions of ion convection and particle precipitation to exciting large-scale traveling atmospheric and ionospheric disturbances. *Journal of Geophysical Research: Space Physics*, *125*(2), e27342. https://doi.org/10.1029/2019JA027342

Shi, X., Zhang, X.-J., Artemyev, A., Angelopoulos, V., Hartinger, M. D., Tsai, E., & Wilkins, C. (2022). On the role of ULF waves in the spatial and temporal periodicity of energetic electron precipitation. *Journal of Geophysical Research: Space Physics*, *127*(12), e2022JA030932. https://doi.org/10.1029/2022JA030932

Shinbori, A., Otsuka, Y., Tsugawa, T., Nishioka, M., Kumamoto, A., Tsuchiya, F., et al. (2021). Relationship between the locations of the midlatitude trough and plasmapause using GNSS TEC and Arase satellite observation data. *Journal of Geophysical Research: Space Physics*, *126*(5), e28943. https://doi.org/10.1029/2020JA028943

Shprits, Y. Y., Subbotin, D. A., Meredith, N. P., & Elkington, S. R. (2008). Review of modeling of losses and sources of relativistic electrons in the outer radiation belt II: Local acceleration and loss. *Journal of Atmospheric and Solar-Terrestrial Physics*, *70*(14), 1694–1713. https://doi.org/10.1016/j.jastp.2008.06.014

Sivadas, N., Semeter, J., Nishimura, Y., & Kero, A. (2017). Simultaneous measurements of substorm-related electron energization in the ionosphere and the plasma sheet. *Journal of Geophysical Research: Space Physics*, *122*(10), 10528–10547. https://doi.org/10.1002/2017JA023995

Sivadas, N., Semeter, J., Nishimura, Y., & Mrak, S. (2019). Optical signatures of the outer radiation belt boundary. *Geophysical Research Letters*, *46*(15), 8588–8596. https://doi.org/10.1029/2019GL083908

SPEDAS. (2023). Space physics environment data analysis software [Software]. SPEDAS. Retrieved from http://spedas.org/wiki/index.php?title=Downloads_and_Installation

Streltsov, A. V., & Bengtson, M. T. (2020). Observations and modeling of whistler mode waves in the magnetospheric density ducts. *Journal of Geophysical Research: Space Physics*, *125*(10), e28398. https://doi.org/10.1029/2020JA028398

Summers, D., & Thorne, R. M. (2003). Relativistic electron pitch-angle scattering by electromagnetic ion cyclotron waves during geomagnetic storms. *Journal of Geophysical Research*, *108*(A4), 1143. https://doi.org/10.1029/2002JA009489

TEC. (2023). Madrigal database of total electron content (TEC) [Dataset]. TEC. Retrieved from http://cedar.openmadrigal.org

Thorne, R. M., Bortnik, J., Li, W., & Ma, Q. (2021). Wave–particle interactions in the earth's magnetosphere. In *Magnetospheres in the solar system* (pp. 93–108). American Geophysical Union (AGU). https://doi.org/10.1002/9781119815624.ch6

Thorne, R. M., & Kennel, C. F. (1971). Relativistic electron precipitation during magnetic storm main phase. *Journal of Geophysical Research*, *76*(19), 4446–4453. https://doi.org/10.1029/JA076i019p04446

Thorne, R. M., Ni, B., Tao, X., Horne, R. B., & Meredith, N. P. (2010). Scattering by chorus waves as the dominant cause of diffuse auroral precipitation. *Nature*, *467*(7318), 943–946. https://doi.org/10.1038/nature09467

Tsai, E., Artemyev, A., Zhang, X.-J., & Angelopoulos, V. (2022). Relativistic electron precipitation driven by nonlinear resonance with whistler-mode waves. *Journal of Geophysical Research: Space Physics*, *127*(5), e30338. https://doi.org/10.1029/2022JA030338

Tsyganenko, N. A. (1995). Modeling the Earth's magnetospheric magnetic field confined within a realistic magnetopause. *Journal of Geophysical Research*, *100*(A4), 5599–5612. https://doi.org/10.1029/94JA03193

Turner, D. L., Shprits, Y., Hartinger, M., & Angelopoulos, V. (2012). Explaining sudden losses of outer radiation belt electrons during geomagnetic storms. *Nature Physics*, *8*(3), 208–212. https://doi.org/10.1038/nphys2185

Vierinen, J., Coster, A. J., Rideout, W. C., Erickson, P. J., & Norberg, J. (2015). Statistical framework for estimating GNSS bias. *Atmospheric Measurement Techniques Discussions*, *8*(9), 9373–9398. https://doi.org/10.5194/amtd-8-9373-2015

Vo, H. B., & Foster, J. C. (2001). A quantitative study of ionospheric density gradients at midlatitudes. *Journal of Geophysical Research*, *106*(A10), 21555–21564. https://doi.org/10.1029/2000JA000397

Walsh, B. M., Foster, J. C., Erickson, P. J., & Sibeck, D. G. (2014). Simultaneous ground- and space-based observations of the plasmaspheric plume and reconnection. *Science*, *343*(6175), 1122–1125. https://doi.org/10.1126/science.1247212

Watt, C. E. J., Degeling, A. W., & Rankin, R. (2013). Constructing the frequency and wave normal distribution of whistler-mode wave power. *Journal of Geophysical Research*, *118*(5), 1984–1991. https://doi.org/10.1002/jgra.50231

Weygand, J. M., Zhelavskaya, I., & Shprits, Y. (2021). A comparison of the location of the mid latitude trough and plasmapause boundary. *Journal of Geophysical Research: Space Physics*, *126*(4), e28213. https://doi.org/10.1029/2020JA028213

Wilkins, C., Angelopoulos, V., Runov, A., Artemyev, A., Zhang, X.-J., Liu, J., & Tsai, E. (2023). Statistical characteristics of the electron isotropy boundary. arXiv e-prints, arXiv:2305.16260.

Woodroffe, J. R., & Streltsov, A. V. (2013). Whistler propagation in the plasmapause. *Journal of Geophysical Research: Space Physics*, *118*(2), 716–723. https://doi.org/10.1002/jgra.50135

Xu, W., Marshall, R. A., Tyssøy, H. N., & Fang, X. (2020). A generalized method for calculating atmospheric ionization by energetic electron precipitation. *Journal of Geophysical Research: Space Physics*, *125*(11), e28482. https://doi.org/10.1029/2020JA028482

Yizengaw, E., & Moldwin, M. B. (2005). The altitude extension of the mid-latitude trough and its correlation with plasmapause position. *Geophysical Research Letters*, *32*(9), L09105. https://doi.org/10.1029/2005GL022854

Zhang, X.-J., Angelopoulos, V., Artemyev, A., Mourenas, D., Agapitov, O., Tsai, E., & Wilkins, C. (2023). Temporal scales of electron precipitation driven by whistler-mode waves. *Journal of Geophysical Research: Space Physics*, *128*(1), e2022JA031087. https://doi.org/10.1029/2022JA031087

Zhang, X.-J., Artemyev, A., Angelopoulos, V., Tsai, E., Wilkins, C., Kasahara, S., et al. (2022). Superfast precipitation of energetic electrons in the radiation belts of the Earth. *Nature Communications*, *13*(1), 1611. https://doi.org/10.1038/s41467-022-29291-8